ACS Catalysis

Research Article

pubs.acs.org/acscatalysis

Influence of Passivation on the Reactivity of Unpromoted and Rb-Promoted Mo_2C Nanoparticles for CO Hydrogenation

Heng Shou,[†] Daniela Ferrari,[‡] David G. Barton,[§] Christopher W. Jones,[⊥] and Robert J. Davis[†,*]

[†]Department of Chemical Engineering, University of Virginia, 102 Engineers' Way, P.O. Box 400741, Charlottesville, Virginia 22904-4741, United States

[‡]The Dow Chemical Company, Freeport, Texas 77541, United States

[§]The Dow Chemical Company, Midland, Michigan 48674, United States

[⊥]School of Chemical & Biomolecular Engineering, Georgia Institute of Technology, 311 Ferst Drive, Atlanta, Georgia 30332, United States

ABSTRACT: Unpromoted and Rb-promoted Mo_2C nanoparticles (~1 nm in size) were synthesized on α-alumina and used for CO hydrogenation. The reaction was performed in a fixed-bed reactor system operating at 573 K and 30 bar with a gas flow rate of 24,000 $cm^3\ g_{Mo}^{-1}\ h^{-1}$ and H_2/CO ratio of 1:1. Unpromoted Mo_2C functioned as a Fischer–Tropsch catalyst producing mostly hydrocarbons at the standard conditions. Passivation of freshly synthesized Mo_2C nanoparticles in 1% O_2 prior to CO hydrogenation decreased the Fischer–Tropsch activity of the catalyst by about 40% compared with a nonpassivated sample. Addition of Rb promoter to Mo_2C shifted the selectivity of the catalyst by inhibiting the formation of hydrocarbons while preserving the formation of alcohols. The presence of Rb with Mo_2C also reduced substantially the sensitivity of the catalyst to passivation by 1% O_2 compared with unpromoted Mo_2C. The partial oxidation of the Mo_2C nanoparticles by passivation and partial reduction by syngas was confirmed by Mo *K* edge X-ray absorption spectroscopy.

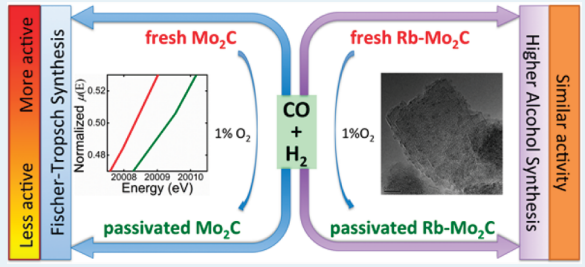

KEYWORDS: *molybdenum carbide, passivation effect, CO hydrogenation, X-ray absorption spectroscopy, ethanol, propanol*

INTRODUCTION

Limited crude oil reserves and competition with the food industry associated with fermentation-based biofuel production inspire new efforts on effective catalytic transformations of alternative carbon sources to produce energy carriers and chemical feedstocks. Production of higher alcohols from the catalytic conversion of synthesis gas (CO + H_2) derived from coal, natural gas, or renewable biomass is one strategy that has shown some promise.[1−4]

Although Rh-based catalysts are effective for the formation of ethanol and other C2-oxygenates from syngas,[5−7] the very high cost of Rh likely prohibits its large scale utilization. Several nonprecious metal catalysts for higher alcohol synthesis have thus been evaluated and include, for example, MoS_2, Cu–Co, Cu–Zn–Al, and Zn–Cr–K, but improvements in the overall catalytic activity, alcohol selectivity, and long-term stability of these materials are still needed.[2]

Early transition metal carbides are also recognized as potential substitutes to precious metal catalysts because of their similar surface electronic properties.[8−10] For example, molybdenum carbide catalysts are well-known to produce hydrocarbons from syngas via Fischer–Tropsch synthesis,[11−13] but the selectivity of the reaction shifts from hydrocarbons to higher alcohols when appropriate promoters and reaction conditions are used.[14,15] The highly reactive carbide surface is very sensitive to oxygen and therefore needs to be passivated before exposure to air.

Prior works have described the various behaviors of oxygen-modified carbide surfaces in different reactions. For example, Ribeiro et al. and Iglesia et al. claimed that surface oxygen inhibits the very high reactivity of fresh tungsten carbide for hydrogenolysis of hydrocarbons. However, partial oxidation of the tungsten carbide surface also forms acid sites that catalyze hydrocarbon isomerization reactions through coupled dehydrogenation and carbenium ion reactions.[16−20] For a reaction such as higher alcohol synthesis from syngas, the presence of acid sites on the catalyst formed by passivation would likely be detrimental to the desired product distribution. In other work, Liu et al. reported that a carbide-modified W(111) surface was highly selective for the dehydrogenation of cyclohexane to benzene after exposure to O_2 at 900 K, but was inactive to cyclohexane after exposure to O_2 at <600 K.[21] Similarly, Hwu et al. found that a carbide-modified Mo(110) surface exposed to O_2 at 900 K exhibited decomposition activity for cyclohexene, ethylene, and methanol, whereas the carbide surface was relatively unreactive toward those substrates after O_2 exposure

Received: February 1, 2012
Revised: May 22, 2012
Published: May 28, 2012

at 600 K.[22] Nagai et al. also showed that passivation of molybdenum carbide with dilute O_2 at room temperature reduced its activity in CO_2 hydrogenation to form CO and CH_4.[23] Using FT-IR spectroscopy, Wu et al. revealed that a surface passivation procedure with dilute O_2 at room temperature irreversibly modified a fresh molybdenum carbide surface, hence, significantly reducing the number of sites for CO adsorption.[24,25]

Evidently, carbidic carbon atoms or metal atoms react with the O_2 used in passivation, which can significantly modify the observed reactivity of carbide catalysts. Therefore, the influence of O_2 on reactivity must be examined as part of any comprehensive study of carbidic materials for catalysis. In this work, the influence of passivation on the structure and CO hydrogenation activity of alumina-supported Mo_2C catalysts, with and without alkali metal promoter, was explored.

EXPERIMENTAL METHODS

1. Catalyst Synthesis. Incorporation of Mo onto the alumina support (Mager Scientific, >99.98%, predominantly α-phase, S_{BET} = 26.8 m^2 g^{-1}) was accomplished by incipient wetness impregnation of an aqueous solution of $(NH_4)_6Mo_7O_{24}{\cdot}4H_2O$ (99.98%, Aldrich) followed by drying in air for 12 h at 400 K and calcining in flowing air for 5 h at 773 K to produce a supported molybdenum oxide, denoted here as MoO_3/Al_2O_3. The sample of MoO_3/Al_2O_3 was then reduced at 673 K in flowing H_2 (GTS-Welco, 99.999%) for 5 h prior to carburization. The supported oxide sample after reduction is denoted here as MoO_2/Al_2O_3 for reference. (The formation of a partially reduced Mo species is verified by X-ray absorption spectroscopy, reported later.) The partially reduced MoO_2/Al_2O_3 sample was either carburized or promoted with Rb prior to carburization. The Rb-promoted MoO_2/Al_2O_3 samples were prepared by grinding Rb_2CO_3 (99.975%, Alfa Aesar) together with MoO_2/Al_2O_3 in a mortar and pestle. Carburization of MoO_2/Al_2O_3 and Rb-promoted MoO_2/Al_2O_3 was performed in a stainless steel tube reactor (26.7 cm length, 1.27 cm o.d., 0.85 cm i.d.) by heating at a rate of 5 K min^{-1} from room temperature to 673 K and at a rate of 1 K min^{-1} from 673 to 900 K in 11.1 vol % C_2H_6 (GTS-Welco, 99.997%) and 88.9 vol% H_2 (GTS-Welco, 99.999%) at a total gas flow rate of 67.5 cm^3 min^{-1}. After ramping to 900 K in C_2H_6/H_2, the temperature was maintained at 900 K for 8 h. Ethane was used as a carbon source instead of methane to reduce the temperature for carburization,[26,27] since elemental analysis revealed that 74% of the total Rb was vaporized during carburization in CH_4/H_2 at 973 K. The catalyst was subsequently cooled to room temperature in flowing Ar (GTS-Welco, 99.999%, additionally purified by an OMI-2 purifier (Sigma-Aldrich)). The catalysts were used "as carburized" or passivated in a stream of 1.04 vol % O_2/N_2 mixture (GTS-Welco) at room temperature for 12 h. After carburization or passivation, the reactor containing the catalyst was purged with purified flowing Ar, sealed by a cap (Swagelok) on the downstream end and a 3-way valve (Swagelok) on the upstream end, and installed in the high-pressure CO hydrogenation reactor system.

2. Hydrogenation of Carbon Monoxide. Hydrogenation of CO was conducted in a BTRS-Jr. system (Autoclave Engineers) equipped with the fixed-bed stainless steel reactor used to carburize the catalyst. The reactor contained nominally 0.05 g Mo_2C, composed of about 1.0 g of Mo_2C/Al_2O_3 or Rb-promoted Mo_2C/Al_2O_3. The catalysts were tested at identical conditions of 573 K, 30 bar total pressure, syngas (H_2 + CO) flow of 20 cm^3 min^{-1} (STP), and a H_2/CO ratio of 1:1. The reactor was pressurized to 30 bar at room temperature and heated to 573 K before sampling. The catalyst temperature was monitored with a thermocouple in contact with the catalyst bed. The purity of CO (GTS-Welco) was 99.9% and H_2 (GTS-Welco) was 99.999%. In addition, CO was purified by passing it through a silica trap immersed in a dry ice/acetone mixture (195 K) to remove any trace iron carbonyl before introduction to the reactor. The products were analyzed by two Hewlett-Packard 5890 series II gas chromatographs. The first one was equipped with a flame ionization detector and a 50-m-long, HP-1, cross-linked methyl silicone gum capillary column to monitor the formation of hydrocarbons (C1−C10) and alcohols (C1−C7). The second one was equipped with a thermal conductivity detector and a 6-ft-long Alltech-8700 packed column and was used to monitor the formation of CO_2.

According to Burch and Petch,[28] the conversion of CO was derived from the fraction of CO that formed carbon-containing products. The conversion of CO, if low, can be described as

$$\text{conversion}\ (\%) = \sum n_i M_i \times 100/M_{CO}$$

where n_i is the number of carbon atoms in product i, M_i is the percentage of product i detected, and M_{CO} is the percentage of CO in the syngas feed.

The selectivity to product i is based on the total number of carbon atoms in the product and is therefore defined as

$$\text{selectivity}\ (\%) = n_i M_i \times 100/\sum n_i M_i$$

The conversion and selectivities were based on the identified products, which present 93−95% of the total peak area in GC chromatograms.

3. Catalyst Characterization. Elemental analyses of representative samples were performed by Galbraith Laboratories (Knoxville, TN). The loading of molybdenum and rubidium was determined by inductively coupled plasma atomic emission spectroscopy (ICP-AES), and the loading of carbon was evaluated by combustion and coulometric measurement.

Electron microscopy was performed on an FEI Titan transmission electron microscope operated at 200 kV. Two passivated catalysts, 5 wt % Mo_2C/Al_2O_3 and 1.5 wt % Rb−5 wt % Mo_2C/Al_2O_3, were reacted in syngas for 48 h and subsequently passivated again with 1.04 vol % O_2/N_2 (GTS-Welco) at room temperature before TEM analysis. Catalyst powders were dispersed in n-hexane and supported onto a lacey carbon film coated grid. Images were recorded with a Gatan 794 Multi Scan CCD camera.

X-ray absorption spectroscopy (XAS) was performed at the National Synchrotron Light Source (NSLS), Brookhaven National Laboratory. The nonpassivated samples before reaction and all of the samples after reaction were sealed in the reactor and transferred into a glovebox. In the glovebox, all the samples were loaded into borosilicate glass tubes (15 cm length, 0.64 cm o.d., 0.40 cm i.d.) and sealed with silicone plugs on both ends to avoid exposure to air. The sealed glass tubes were further wrapped in parafilm and stored in airtight plastic bags before being taken out of the glovebox. The samples in these sealed tubes were used for ex-situ XAS studies on beamlines X23A2 and X18B at the NSLS. The storage ring was typically operated at 2.8 GeV with a ring current of about 300 mA. The XAS data were obtained in the transmission mode at the Mo K edge (20 keV) with a spot size of 0.5 mm ×3 mm at

dx.doi.org/10.1021/cs300083b | ACS Catal. 2012, 2, 1408−1416

Table 1. Reactivity of Nonpassivated 5 wt % Mo_2C/Al_2O_3 Catalysts in Syngas Reaction[a]

Rb loading (wt %)	0	1.0	1.5	2.0
CO conversion (%)	20	11	5.0	2.6
CO_2 selectivity (%)	47	45	52[b]	42
selectivity (C %, on a CO_2-free basis)				
total hydrocarbons	98	58	44	36
methane	31	16	15	12
C2 hydrocarbons	25	14	11	9.4
C3 hydrocarbons	21	12	7.5	5.8
C4+ linear paraffins	12	7.0	2.8	2.0
C4+ linear olefins	2.1	6.5	5.7	5.1
branched hydrocarbons	5.8	2.3	1.5	1.3
total alcohols	2.4	42	56	64
methanol	1.5	12	16	18
ethanol	0.7	15	21	22
1-propanol	0.3	8.6	12	15
1-butanol	0.0	2.7	4.2	4.6
2-butanol	0.0	1.4	1.0	0.8
C5+ alcohols	0.0	1.7	1.9	4.3
(C2+ alcohols)/(methanol)	0.66	2.5	2.5	2.5
rate of CO consumption (mol_{CO} mol_{Mo}^{-1} h^{-1})	9.9	5.5	2.5	1.3
rate of hydrocarbon production (g g_{Mo}^{-1} h^{-1})	0.80	0.28	0.082	0.044
rate of alcohol production (g g_{Mo}^{-1} h^{-1})	0.037	0.32	0.17	0.12

[a] T = 573 K, P = 30 bar, 0.05 g nominal Mo_2C (~1.0 g supported catalyst), H_2/CO=1, syngas flow =20 cm^3 (STP) min^{-1}. Data were recorded after 48 h reaction. [b] The excess to the theoretical limit (50%) is likely due to a small experimental error.

X-18B and 0.5 mm × 5 mm at X-23A2. The Mo K edge spectra were measured at room temperature with Mo foil (0.015 mm, 99.9%, Goodfellow) as a reference.

The XAS data were processed using the Athena[29,30] software for background removal, postedge normalization, and X-ray absorption near-edge structure (XANES) analysis. Because the Mo near-edge structure has various features that complicate the determination of E_0, the edge energy, the value of E_0 was assigned here as the energy at the half-step height. Metallic Mo foil, MoO_2 (99%, Aldrich), and MoO_3 (99.99%, Aldrich) were used as standards for Mo residing in 0, +4, and +6 formal oxidation states. Standard bulk Mo_2C (Aldrich, 99.5%) was used to determine the amplitude reduction factors, S_0^2, for Mo−C and Mo−Mo. The values of S_0^2 utilized in the fitting of extended X-ray absorption fine structure (EXAFS) data from the catalyst samples were 0.86 and 0.76 for Mo−C and Mo−Mo, respectively. A two-shell fitting procedure was used to analyze Mo carbides (Mo−C, Mo−Mo). The interatomic distances (r), coordination numbers (CN), Debye−Waller factors (σ^2), and energy shifts (ΔE_0) were derived from the fitting results in the Artemis software package.[29]

RESULTS AND DISCUSSION

Although elemental analysis of a 5 wt % Mo_2C/Al_2O_3 catalyst showed a C/Mo molar ratio of 0.39, which is slightly lower than the expected value from stoichiometry (0.5), the EXAFS results discussed later confirmed the formation of a supported carbide. Elemental analysis of a 1.5 wt % Rb−5 wt % Mo_2C/Al_2O_3 revealed a Rb/Mo molar ratio of 0.31, which was close to the nominal value (0.34). Evidently, the low temperature carburization with C_2H_6/H_2 successfully avoided the volatilization of Rb promoter.

The performance of nonpassivated alumina-supported Mo_2C catalysts in the reaction of syngas (CO/H_2 = 1:1) at 573 K and 30 bar pressure is summarized in Table 1. Unpromoted Mo_2C/Al_2O_3 functions primarily as an active Fischer−Tropsch catalyst with 20% CO conversion, producing mainly hydrocarbons (98% on a CO_2-free basis). The addition of 1, 1.5, or 2 wt % Rb_2CO_3 to 5 wt % Mo_2C/Al_2O_3 increased the selectivity to alcohols (42%, 56% or 64%, respectively) at the expense of overall CO conversion (down to 2.6% at the highest promoter loading), which is consistent with our previous study on a Rb-promoted Mo_2C/MgO catalyst[31] and with prior work on potassium-promoted bulk Mo_2C catalysts.[14,15,32] Clearly, there is a trade-off between rate of CO conversion and selectivity to alcohols, as reported earlier.[14,15,31,32]

The change of catalytic performance with time for nonpassivated 1.5 wt % Rb−5 wt % Mo_2C/Al_2O_3 catalyst is presented in Figure 1 as an example. Although the catalyst deactivated continuously over the run, most of the deactivation occurred over the first 20 h, during which the conversion of CO declined by half. Likewise, the major changes in selectivity to hydrocarbons and alcohols occurred during the initial 20 h.

To explore the influence of carburization on the effectiveness of the Rb promoter, dry impregnation of Rb_2CO_3 onto nonpassivated 5 wt % Mo_2C/Al_2O_3 was performed in a glovebox to achieve a 5 wt % Rb−5 wt % Mo_2C/Al_2O_3. The catalytic performance of a 1.5 wt % Rb−5 wt % Mo_2C/Al_2O_3 catalyst prepared with promoter incorporated prior to carburization and the 5 wt % Rb−5 wt % Mo_2C/Al_2O_3 catalyst with promoter impregnated after carburization is compared in Figure 2a and b, respectively. Evidently, when the Rb_2CO_3 promoter was added after carburization (Figure 2b), the catalyst exhibited a negligible initial production rate of alcohols and a relatively high initial production rate of hydrocarbons. However, the production rates varied sharply during the first 8 h of reaction. In contrast, when the Rb_2CO_3 promoter was added before carburization, a relatively steady production rate of alcohols was observed from the beginning of the reaction (Figure 2a). These results are consistent with the mechanism of promotion of MoS_2 and Mo_2C catalysts for CO hydrogenation proposed by Lee et al.,[33,34] which involves the spreading of the

dx.doi.org/10.1021/cs300083b | ACS Catal. 2012, 2, 1408−1416

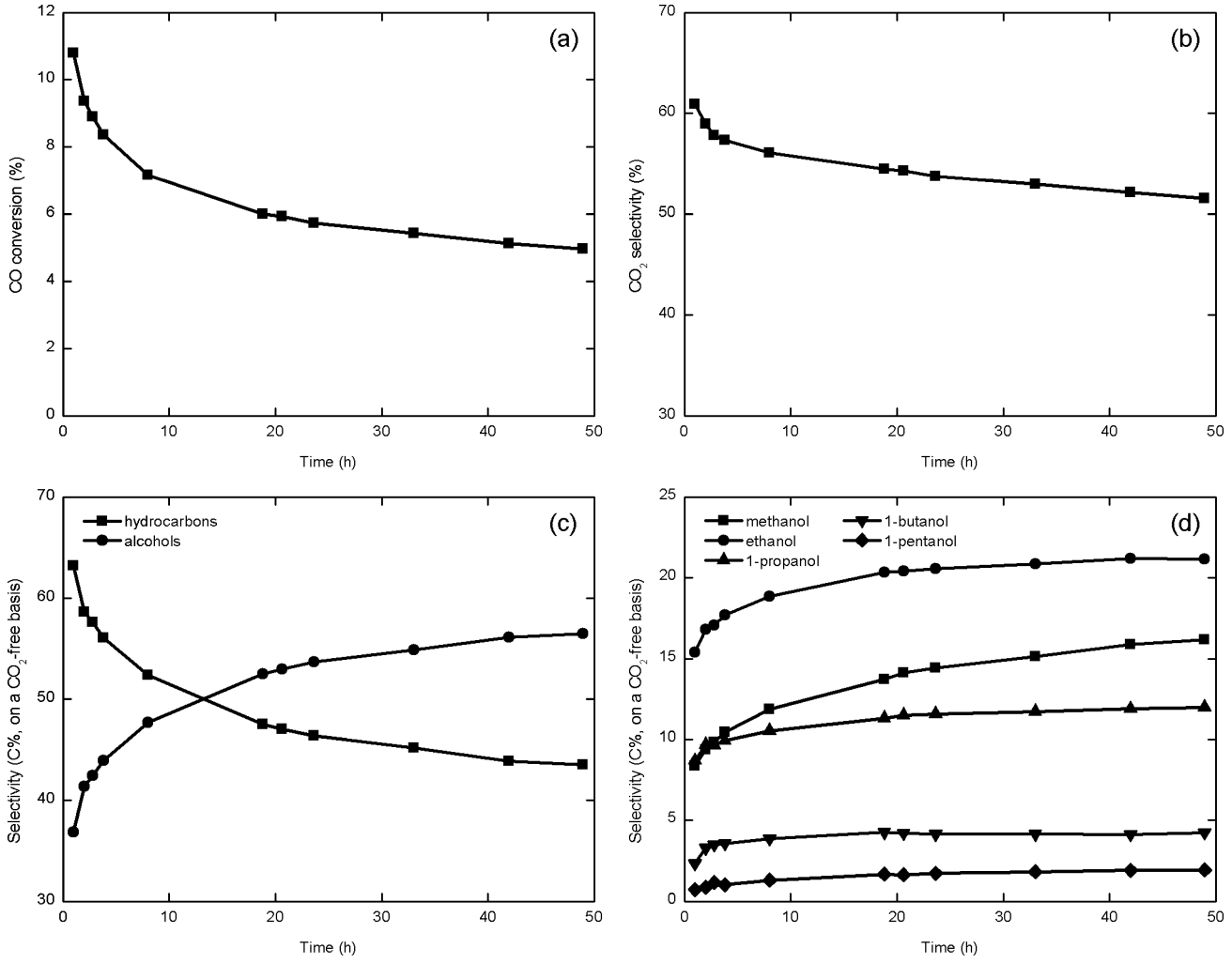

Figure 1. Change in catalytic performance of nonpassivated 1.5 wt % Rb−5 wt % Mo_2C/Al_2O_3 during CO hydrogenation at 573 K and 30 bar over time: (a) CO conversion; (b) selectivity of CO_2; (c) selectivity of total hydrocarbons and of total alcohols; (d) selectivity of C1−C5 linear alcohols.

alkali metal promoter over the active sulfide or carbide at reaction conditions.

For a sample that was promoted prior to carburization (Figure 2a), the carburization treatment at elevated temperature evidently facilitated the effective spreading of the promoter over the catalyst, whereas for a sample promoted after carburization (Figure 2b), at least 8 h of syngas reaction was needed to disperse the Rb promoter. A previous study of Rb-promoted Mo_2C supported on MgO concluded that the structure of bulk Rb_2CO_3 added to the catalyst was altered by exposure to syngas reaction conditions, as observed by Rb K-edge spectroscopy.[31] However, the chemical state of the spreading promoter is not yet known. It is important to note that the production rate of hydrocarbons on the sample that was promoted prior to carburization (Figure 2a) declined by a half over the first 20 h of reaction before reaching a fairly steady rate, whereas the production rate of alcohols deactivated much less severely. The results reported here suggest that although carburization facilitated the spreading of Rb promoter to the active Mo_2C nanoclusters, additional exposure of the catalyst to syngas conditions likely improved the interaction of the promoter with the carbide, which enhanced alcohol selectivity with time on stream during CO hydrogenation.

The influence of passivation on the reactivity of unpromoted and Rb-promoted Mo_2C/Al_2O_3 catalysts can be seen in Table 2. Since we have observed in prior work a strong correlation between CO conversion and hydrocarbon selectivity over supported Mo_2C,[31] a direct comparison of the selectivities requires the same level of CO conversion. Therefore, the loading of unpromoted 5 wt % Mo_2C/Al_2O_3 (nonpassivated and passivated) was adjusted in the reactor to give a conversion of CO at standard conditions comparable with those of the Rb-promoted catalysts. As expected, the unpromoted catalysts produced mainly hydrocarbons, with selectivities of 89 and 98% (on a CO_2-free basis) over the nonpassivated and passivated catalysts, respectively. Passivation decreased the activity of unpromoted 5 wt % Mo_2C/Al_2O_3 catalyst by 37% (reducing the CO consumption rate from 11 to 6.9 mol_{CO} mol_{Mo}^{-1} h^{-1}), indicating a strong influence of surface oxygen on the activity of Mo_2C. This result is reminiscent of the work of Wu et al., who claimed that passivation of Mo_2C with an O_2/N_2 mixture partially oxidized the surface of Mo_2C and irreversibly deactivated most of the sites for CO adsorption.[24,25] The rate of alcohol production over the nonpassivated unpromoted catalyst at low conversion was 0.18 g g_{Mo}^{-1} h^{-1}, which is nearly identical to the alcohol production rate over the promoted catalyst (Table 2), whereas promoter addition decreased the rate of hydrocarbon formation by almost an order of magnitude. These results are similar to those of Tsai et al., who used isotopic transient analysis to probe the promotion of

dx.doi.org/10.1021/cs300083b | ACS Catal. 2012, 2, 1408−1416

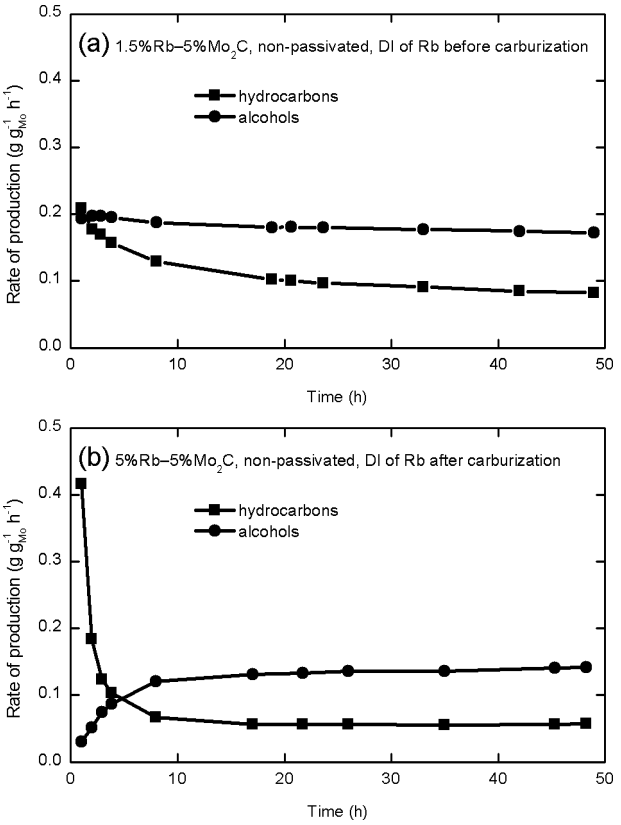

Figure 2. Change in production rates of hydrocarbons (■) and alcohols (●) during CO hydrogenation at 573 K and 30 bar over (a) 1.5 wt % Rb–5 wt % Mo_2C/Al_2O_3, nonpassivated, dry impregnation (DI) of Rb_2CO_3 before carburization and (b) 5 wt % Rb–5 wt % Mo_2C/Al_2O_3, nonpassivated, DI of Rb_2CO_3 after carburization.

a Co-based Fischer–Tropsch catalyst by Cu to form a higher alcohol synthesis catalyst.[35] The addition of Cu promoter significantly decreased the hydrocarbon formation rate on the Co catalyst without affecting the parallel oxygenate synthesis rate, effectively shifting the selectivity of the catalyst from hydrocarbons to oxygenates. Although the total alcohol production rate over nonpassivated Mo_2C was essentially unchanged by the addition of 1.5 wt % Rb (Table 2), the ratio of higher alcohols to methanol (from carbon-based selectivity at constant CO conversion) increased from 1.2 to 2.5 by addition of the promoter. However, the alcohol production rate over an unpromoted catalyst was severely reduced from 0.18 to 0.017 g g_{Mo}^{-1} h^{-1} by passivation, which is additional evidence of an irreversible surface modification of Mo_2C by oxygen. On the other hand, passivation had only a negligible influence on the activity of Rb-promoted 5 wt % Mo_2C/Al_2O_3 catalyst (Table 2), indicating that interactions of the Mo_2C with the alkali metal promoter dominate the surface reactivity over that of added oxygen. It should be noted that the selectivity to CO_2, presumably via the water-gas-shift reaction, was high in all cases (~40–50%), regardless of passivation or promotion. According to reaction stoichiometry, the maximum selectivity to CO_2 cannot exceed 50%.

The chain growth probability (α) based on the C1–C6 linear hydrocarbons (paraffins and olefins combined) was calculated from the Anderson–Schulz–Flory (ASF) distribution, expressed as

$$W_n/n = (1 - \alpha)^2\alpha^{n-1}$$

Table 2. Influence of Passivation on the Reactivity of Unpromoted and Rb-Promoted 5 wt % Mo_2C/Al_2O_3 Catalysts at Similar CO Conversion Levels[a]

Rb loading (wt %)	0		1.5	
passivation	no	yes	no	yes
syngas flow rate (cm^3 g_{Mo}^{-1} h^{-1})	96 000	53 000	24 000	24 000
CO conversion (%)	5.6	5.5	5.0	4.7
CO_2 selectivity (%)	46	48	52[b]	44
selectivity (C %, on a CO_2-free basis)				
total hydrocarbons	89	98	44	47
methane	33	45	15	18
C2 hydrocarbons	24	27	11	13
C3 hydrocarbons	17	17	7.5	7.9
C4+ linear paraffins	6.5	4.4	2.8	2.4
C4+ linear olefins	2.0	1.3	5.7	4.4
branched hydrocarbons	7.0	4.3	1.5	1.3
total alcohols	11	1.6	56	53
methanol	4.9	0.89	16	16
ethanol	4.1	0.70	21	19
1-propanol	1.8	0.0	12	12
1-butanol	0.0	0.0	4.2	3.8
2-butanol	0.0	0.0	1.0	0.8
1-pentanol	0.0	0.0	1.9	1.6
(C2+ alcohols)/(methanol)	1.2	0.79	2.5	2.4
rate of CO consumption (mol_{CO} mol_{Mo}^{-1} h^{-1})	11	6.9	2.5	2.3
rate of hydrocarbon production (g g_{Mo}^{-1} h^{-1})	0.85	0.57	0.082	0.098
rate of alcohol production (g g_{Mo}^{-1} h^{-1})	0.18	0.017	0.17	0.17

[a] T = 573 K, P = 30 bar, H_2/CO = 1. Data were recorded after 48 h reaction. [b] The excess beyond the theoretical limit (50%) is likely due to experimental error in analysis.

where W_n is the weight fraction of hydrocarbon molecules containing n carbon atoms among all the hydrocarbons considered. After transforming the ASF distribution to

$$\log(W_n/n) = (n - 1)\log\alpha + 2\log(1 - \alpha)$$

the value of α can be determined from the linear fit shown in Figure 3. The resulting chain growth probabilities are summarized in Table 3. Neither passivation nor Rb promoter

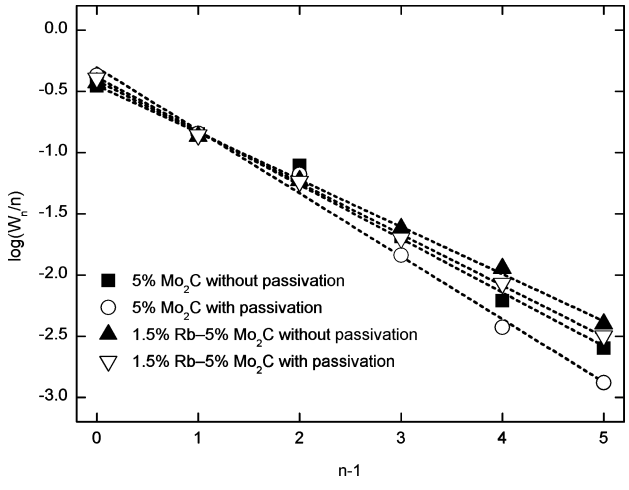

Figure 3. Evaluation of chain growth probability of linear hydrocarbons (paraffins and olefins combined).

dx.doi.org/10.1021/cs300083b | ACS Catal. 2012, 2, 1408–1416

had a significant influence on the value of hydrocarbon chain growth probability, which varied from 0.31 to 0.41.

Table 3. Chain Growth Probability of Hydrocarbons (Paraffins and Olefins Combined)

sample	chain growth probability
5 wt % Mo_2C/Al_2O_3 without passivation	0.36
5 wt % Mo_2C/Al_2O_3 with passivation	0.31
1.5 wt % Rb−5 wt % Mo_2C/Al_2O_3 without passivation	0.41
1.5 wt % Rb−5 wt % Mo_2C/Al_2O_3 with passivation	0.38

The X-ray absorption near-edge structure (XANES) at the Mo K edge of reference compounds and catalysts is summarized in Figure 4 and Table 4. The shift in the edge position, determined at half-step height, is defined as the increase of E_0 value from that of the metallic Mo foil. The

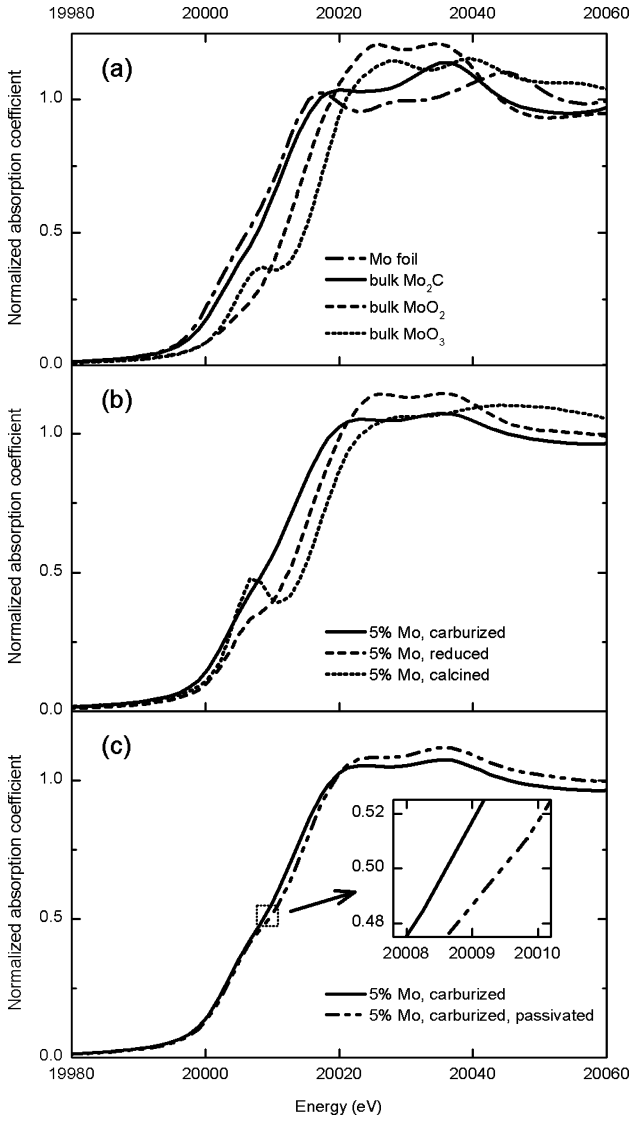

Figure 4. XANES at the Mo K edge of (a) Mo reference standards, (b) alumina-supported Mo species, MoO_3/Al_2O_3 (calcined), MoO_2/Al_2O_3 (reduced), and Mo_2C/Al_2O_3 (carburized); (c) a comparison between freshly prepared and passivated Mo_2C/Al_2O_3.

Table 4. Shift of the Mo K Edge Energy from Mo Foil

Mo samples		shift of E_0 (eV)
Mo foil		0.0
MoO_2		5.6
MoO_3		8.5
bulk Mo_2C		1.5
5% Mo/Al_2O_3, calcined		8.2
5% Mo/Al_2O_3, reduced		6.2
1.5% Rb−5% Mo/Al_2O_3, reduced		6.7
5% Mo_2C/Al_2O_3 without passivation	before rxn	2.4
	after rxn	2.3
5% Mo_2C/Al_2O_3 with passivation	before rxn	3.3
	after rxn	2.8
1.5% Rb−5% Mo_2C/Al_2O_3 without passivation	before rxn	2.8
	after rxn	2.2
1.5% Rb−5% Mo_2C/Al_2O_3 with passivation	before rxn	3.1
	after rxn	2.9

calcined alumina-supported Mo species had a similar K edge energy shift (8.2 eV) to that of the Mo(VI) standard, MoO_3 (8.5 eV). After reduction in H_2, the energy shift of E_0 for the alumina-supported Mo species was significantly decreased to 6.2 eV, which is close to that of Mo(IV) in MoO_2 (5.6 eV shift). The addition of Rb promoter did not significantly change the energy shift for MoO_2/Al_2O_3. Carburization of MoO_2/Al_2O_3 and Rb-promoted Mo_2C further reduced the Mo oxidation state, resulting in an E_0 shift of 2.4 eV for Mo_2C/Al_2O_3, which approaches that of bulk Mo_2C (1.5 eV). However, nonpassivated Mo_2C/Al_2O_3 still was more oxidized than bulk Mo_2C, which may be attributed to incomplete carburization of the highly dispersed Mo_2C clusters, the interaction of Mo with the underlying support, or both.

According to the shifts in E_0 reported in Table 4, both passivation and addition of Rb promoter resulted in partial oxidation of the Mo_2C clusters. For example, a nonpassivated sample of Mo_2C/Al_2O_3 before reaction had an E_0 shift of 2.4 eV relative to Mo foil, whereas a passivated sample had an E_0 shift of 3.3 eV. The difference between the E_0 of the nonpassivated 1.5 wt % Rb−5 wt % Mo_2C/Al_2O_3 sample (2.8 eV) and the corresponding passivated one (3.1 eV) suggests that the presence of Rb promoter inhibited oxidation of the carbide surface. The shifts in E_0 caused by the CO hydrogenation reaction that are reported in Table 4 confirmed that the supported Mo_2C clusters (with and without passivation, with and without promoter) can be reduced by the reactive syngas environment, which is consistent with the observation on a Rb-promoted Mo_2C/MgO catalyst.[31] The very small difference in E_0 (0.1 eV) before and after reaction of nonpassivated 5 wt % Mo_2C/Al_2O_3 confirmed the success of our air-free handling of the samples.

The structural evolution of the Mo phase during catalyst synthesis can be followed in the Mo K edge extended X-ray absorption fine structure (EXAFS). Thus, Fourier transforms (FT) of the k^3-weighted EXAFS of the samples at various stages of the synthesis procedure were compared with those of the reference bulk compounds. According to the EXAFS in Figure 5a and the shift in E_0 in Table 4, the alumina-supported Mo oxide after calcination is a highly dispersed Mo(VI) oxide with no clear evidence of a Mo−Mo shell. After reduction in H_2, the FT of the EXAFS of alumina-supported Mo oxide (Figure 5c and d) and the shift in E_0 reported in Table 4 suggested the

dx.doi.org/10.1021/cs300083b | ACS Catal. 2012, 2, 1408−1416

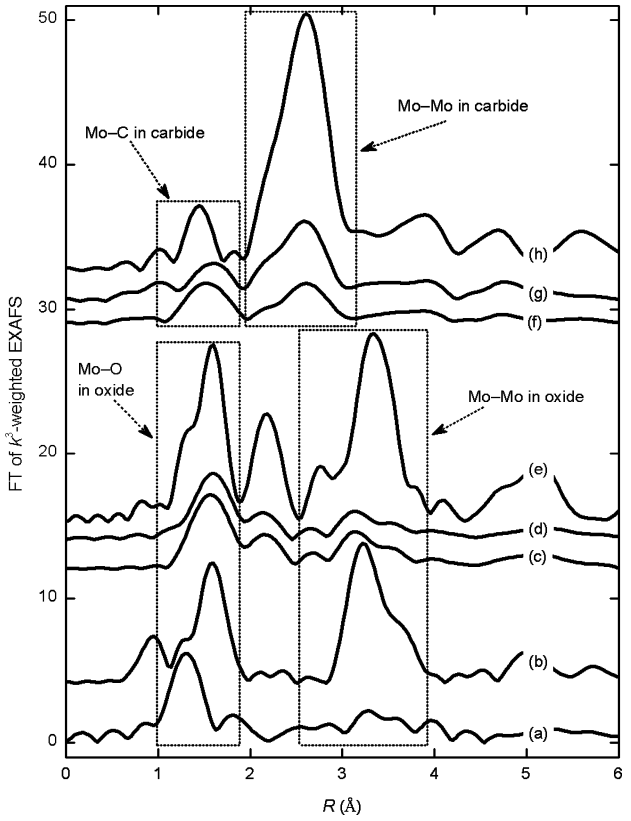

Figure 5. Fourier transform (not corrected for phase shifts) of k^3-weighted Mo EXAFS: (a) 5% Mo/Al_2O_3, calcined; (b) bulk MoO_3; (c) 5 wt % Mo/Al_2O_3, reduced; (d) 1.5 wt % Rb–5 wt % Mo/Al_2O_3, reduced; (e) bulk MoO_2; (f) 5 wt % Mo, carburized; (g) 1.5 wt % Rb–5 wt % Mo, carburized; and (h) bulk Mo_2C. Spectra are offset for clarity.

formation of a highly dispersed Mo suboxide, likely Mo(IV), as an intermediate during the catalyst synthesis procedure. After carburization, the FT of the EXAFS of both unpromoted (Figure 5f) and Rb-promoted (Figure 5g) samples revealed a Mo–Mo shell at the same position as the one in bulk Mo_2C (Figure 5h), which confirmed the formation of alumina-supported Mo_2C. Kojima and Aika reported that when Cs was added onto a MoO_3 precursor prior to carburization, the final material tended to form metallic Mo rather than carbidic Mo;[36] however, our procedure involving the addition of Rb promoter prior to carburization was able to produce supported Mo carbide rather than metallic Mo.

The coordination numbers, interatomic distances, and Debye–Waller factors obtained by curve-fitting of the k^3-weighted EXAFS of the carbide samples are summarized in Table 5. The number of reliable parameters that can be measured is limited by the Nyquist theorem, given here as $2\Delta k\Delta R/\pi = 15$, and exceeds the number of fitted parameters reported in Table 5. In addition, the R factors in Table 5 are all smaller than 0.07. A sample of the results from curve-fitting of 1.5 wt % Rb–5 wt % Mo_2C/Al_2O_3 (without passivation, before reaction) is provided in Figure 6 to illustrate the quality of the fits.

The low Mo–Mo coordination numbers (2.5–5.2) indicate that the Mo carbide clusters are very highly dispersed on the alumina support, which is consistent with the average particle size of ~1 nm, as observed by electron microscopy (Figure 7). The formation of very highly dispersed Mo_2C clusters has also been observed on H-ZSM-5 zeolite[37] and γ-Al_2O_3,[38] with Mo–Mo coordination numbers derived from EXAFS as low as 2.6 and 4, respectively.

CONCLUSIONS

A modified catalyst synthesis method for preparing alkali-promoted supported Mo_2C was developed, with the incorporation of alkali metal promoter accomplished prior to carburization. The new procedure gives 1 nm Mo_2C nanoparticles supported on α-alumina. An unpromoted sample of Mo_2C/Al_2O_3 was active in the Fischer–Tropsch reaction and produced mostly hydrocarbons with a chain growth probability of ~0.36, whereas addition of Rb shifted the selectivity to alcohols, primarily by inhibiting the rate of hydrocarbon formation. However, increasing the loading of Rb promoter beyond 1 wt % decreased the rate of alcohol production, presumably because of blockage of the active sites for alcohol synthesis. The primary role of Rb on the supported carbide clusters appears to be the deactivation of sites used to form hydrocarbons, although we cannot rule out a promotion of higher alcohol synthesis rates on the carbide surfaces or catalysis of alcohol coupling reactions. Passivation of unpromoted 5 wt % Mo_2C/Al_2O_3 with a dilute stream of O_2 decreased the overall activity of the catalyst by 37% and reduced the rate of alcohol production by an order of magnitude, whereas passivation of promoted (1.5 wt % Rb) 5 wt % Mo_2C/Al_2O_3 did not significantly affect the activity and

Table 5. Results from the Analysis of Mo EXAFS from Carbide Catalyst[a]

catalyst[b]	shell	CN	r (Å)	$\Delta\sigma^2$ (10^{-3} Å^2)	ΔE_0 (eV)	R factor
bulk Mo_2C	Mo–C	3[c]	2.11 ± 0.03	3.4 ± 3.4	0.9 ± 5.0	0.009
	Mo–Mo	12[c]	2.97 ± 0.01	5.6 ± 0.7	−7.8 ± 1.1	
5 wt % Mo_2C/Al_2O_3 without passivation	Mo–C	3.3 ± 0.8	2.12 ± 0.02	5.8 ± 2.3	−3.2 ± 3.1	0.047
	Mo–Mo	2.5 ± 0.9	2.98 ± 0.01	7.8 ± 2.1	−5.4 ± 3.0	
5 wt % Mo_2C/Al_2O_3 with passivation[d]	Mo–C	1.8 ± 0.8	2.05 ± 0.02	0.0 ± 2.6	−24 ± 8	0.066
	Mo–Mo	2.8 ± 1.1	2.98 ± 0.02	6.6 ± 2.4	−7.5 ± 3.6	
1.5 wt % Rb–5 wt % Mo_2C/Al_2O_3 without passivation[d]	Mo–C	2.2 ± 1.2	2.11 ± 0.03	1.9 ± 3.8	−11 ± 8	0.053
	Mo–Mo	5.2 ± 1.7	2.97 ± 0.01	7.2 ± 1.9	−13 ± 3	
1.5 wt % Rb–5 wt % Mo_2C/Al_2O_3 with passivation[d]	Mo–C	1.8 ± 1.1	2.08 ± 0.03	3.0 ± 3.4	−22 ± 10	0.061
	Mo–Mo	4.6 ± 1.6	2.97 ± 0.01	7.3 ± 2.0	−13 ± 3	

[a]Fitting parameters: Fourier transform range, Δk, 2–11.8 Å^{-1}; fitting range, ΔR, 1–3.4 Å; weighting, k^3, S_0^2 (Mo–C) = 0.86, S_0^2 (Mo–Mo) = 0.76. [b]Catalysts are all before reaction. [c]Value was assigned in curving-fitting on the basis of standard structure. [d]R_{bkg} was set to 1.2 in background removal to remove the noise oscillation below 1 Å in R space.

dx.doi.org/10.1021/cs300083b | ACS Catal. 2012, 2, 1408–1416

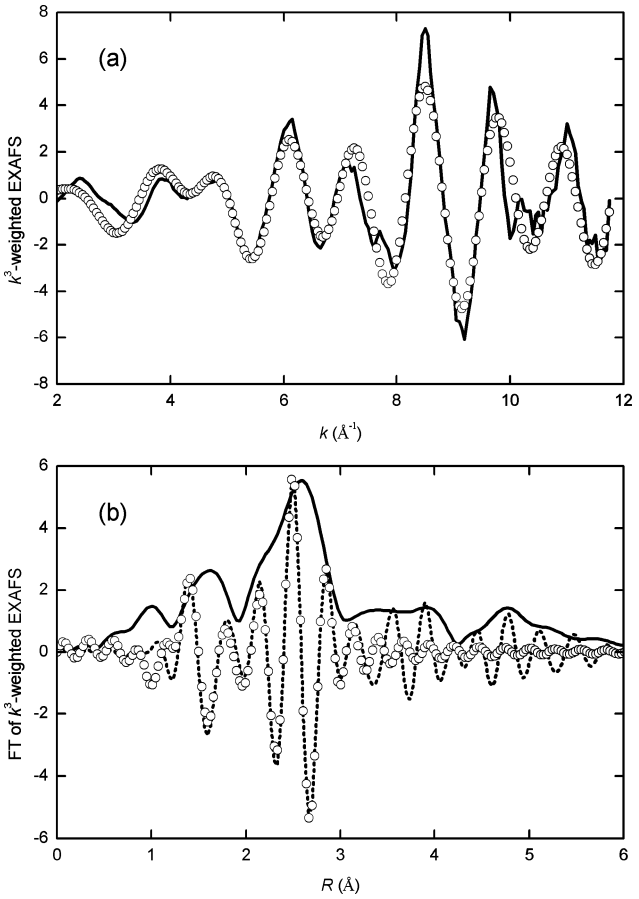

Figure 6. Comparison of the curve fit to experimental Mo K edge EXAFS of the 1.5 wt % Rb−5 wt % Mo_2C/Al_2O_3 catalyst without passivation, before reaction. (a) k^3-Weighted Mo K edge EXAFS (solid line) and the result from curve fit (circles); (b) magnitude (solid line) and the imaginary part (dashed line) of the Fourier transform of EXAFS compared with the result from the curve fit (circles).

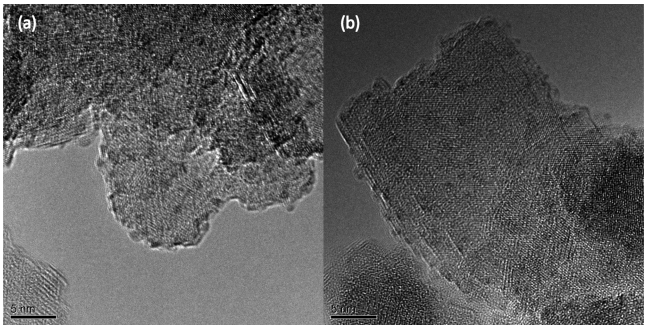

Figure 7. Electron micrographs of (a) 5 wt % Mo_2C/Al_2O_3 with passivation after reaction, (b) 1.5 wt % Rb−5 wt % Mo_2C/Al_2O_3 with passivation and after reaction. Catalysts were used for 48 h in CO hydrogenation before TEM analysis. The scale bars are 5 nm.

product distribution of the catalyst. Spectroscopic characterization at Mo K edge was used to follow the evolution of the structure of the catalyst throughout the synthesis procedure as well as to monitor the partial oxidation and reduction of the carbide catalysts during passivation and CO hydrogenation, respectively. The Mo XANES confirmed the reduction of Mo(VI) to Mo(IV) to Mo_2C; however, the supported Mo_2C was always partially oxidized compared with bulk Mo_2C.

AUTHOR INFORMATION

Corresponding Author

*Phone: +14349246284. Fax: +14349822658. E-mail: rjd4f@virginia.edu.

Notes

The authors declare no competing financial interest.

ACKNOWLEDGMENTS

The authors acknowledge financial support from The Dow Chemical Company and helpful discussions with collaborators Dr. Pradeep Agrawal, Dr. David Sholl, and Mr. Michael Morrill at the Georgia Institute of Technology. The authors also acknowledge Mr. Richard White at University of Virginia for acquisition of the transmission electron micrographs. Use of the NSLS was supported by the US Department of Energy, Office of Science, Office of Basic Energy Sciences, under Contract No. DE-AC02-98CH10886. Beamline X18B at the NSLS is supported in part by the Synchrotron Catalysis Consortium, US Department of Energy Grant No. DE-FG02-05ER15688. The authors acknowledge with gratitude the invaluable assistance received from the X-23A2 beamline personnel, Dr. Bruce Ravel, and the X-18B beamline personnel, Dr. Nebojsa Marinkovic, and Dr. Syed Khalid.

REFERENCES

(1) Forzatti, P.; Tronconi, E.; Pasquon, I. *Catal. Rev. Sci. Eng.* **1991**, *33*, 109−168.
(2) Wender, I. *Fuel Process. Technol.* **1996**, *48*, 189−297.
(3) Herman, R. G. *Catal. Today* **2000**, *55*, 233−245.
(4) Fang, K.; Li, D.; Lin, M.; Xiang, M.; Wei, W.; Sun, Y. *Catal. Today* **2009**, *147*, 133−138.
(5) Bhasin, M. M.; O'Connor, G. L. Belgian Patent 824822, 1975.
(6) Spivey, J. J.; Egbebi, A. *Chem. Soc. Rev.* **2007**, *36*, 1514−1528.
(7) Subramani, V.; Gangwal, S. K. *Energy Fuels* **2008**, *22*, 814−839.
(8) Levy, R. B.; Boudart, M. *Science* **1973**, *181*, 547−549.
(9) Chen, J. G. *Chem. Rev.* **1996**, *96*, 1477−1498.
(10) Hwu, H. H.; Chen, J. G. *Chem. Rev.* **2005**, *105*, 185−212.
(11) Park, K. Y.; Seo, W. K.; Lee, J. S. *Catal. Lett.* **1991**, *11*, 349−356.
(12) Vo, D.-V. N.; Adesina, A. A. *Appl. Catal., A* **2011**, *399*, 221−232.
(13) Vo, D.-V. N.; Nguyen, T.-H.; Kennedy, E. M.; Dlugogorski, B. Z.; Adesina, A. A. *Catal. Today* **2011**, *175*, 450−459.
(14) Woo, H. C.; Park, K. Y.; Kim, Y. G.; Nam, I. S.; Chung, J. S.; Lee, J. S. *Appl. Catal* **1991**, *75*, 267−280.
(15) Xiang, M.; Li, D.; Li, W.; Zhong, B.; Sun, Y. *Fuel* **2006**, *85*, 2662−2665.
(16) Ribeiro, F. H.; Dalla Betta, R. A.; Boudart, M.; Baumgartner, J.; Iglesia, E. *J. Catal.* **1991**, *130*, 86−105.
(17) Ribeiro, F. H.; Boudart, M.; Dalla Betta, R. A.; Iglesia, E. *J. Catal.* **1991**, *130*, 498−513.
(18) Iglesia, E.; Baumgartner, J. E.; Ribeiro, F. H.; Boudart, M. *J. Catal.* **1991**, *131*, 523−544.
(19) Iglesia, E.; Ribeiro, F. H.; Boudart, M.; Baumgartner, J. E. *Catal. Today* **1992**, *15*, 307−337.
(20) Iglesia, E.; Ribeiro, F. H.; Boudart, M.; Baumgartner, J. E. *Catal. Today* **1992**, *15*, 455−458.
(21) Liu, N.; Rykov, S. A.; Chen, J. G. *Surf. Sci.* **2001**, *487*, 107−117.
(22) Hwu, H. H.; Zellner, M. B.; Chen, J. G. *J. Catal.* **2005**, *229*, 30−44.
(23) Nagai, M.; Kurakami, T.; Omi, S. *Catal. Today* **1998**, *45*, 235−239.
(24) Wu, W.; Wu, Z.; Liang, C.; Chen, X.; Ying, P.; Li, C. *J. Phys. Chem. B* **2003**, *107*, 7088−7094.
(25) Wu, W.; Wu, Z.; Liang, C.; Ying, P.; Feng, Z.; Li, C. *Phys. Chem. Chem. Phys.* **2004**, *6*, 5603.
(26) Li, S.; Kim, W. B.; Lee, J. S. *Chem. Mater.* **1998**, *10*, 1853−1862.

(27) Claridge, J. B.; York, A. P. E.; Brungs, A. J.; Green, M. L. H. *Chem. Mater.* **2000**, *12*, 132−142.
(28) Burch, R.; Petch, M. I. *Appl. Catal., A* **1992**, *88*, 39−60.
(29) Ravel, B.; Newville, M. *J. Synchrotron Radiat.* **2005**, *12*, 537−541.
(30) Zabinsky, S. I.; Rehr, J. J.; Ankudinov, A.; Albers, R. C.; Eller, M. J. *Phys. Rev. B* **1995**, *52*, 2995−3009.
(31) Shou, H.; Davis, R. J. *J. Catal.* **2011**, *282*, 83−93.
(32) Kim, H. G.; Lee, K. H.; Lee, J. S. *Res. Chem. Intermed.* **2000**, *26*, 427.
(33) Tsai, Y.-T.; Mo, X.; Goodwin, J. G., Jr. *J. Catal.* **2012**, *285*, 242−250.
(34) Lee, J. S.; Kim, S.; Lee, K. H.; Nam, I.-S.; Chung, J. S.; Kim, Y. G.; Woo, H. C. *Appl. Catal., A* **1994**, *110*, 11−25.
(35) Lee, J. S.; Kim, S.; Kim, Y. G. *Top. Catal.* **1995**, *2*, 127−140.
(36) Kojima, R.; Aika, K. *Appl. Catal., A* **2001**, *219*, 141−147.
(37) Ding, W.; Li, S.; Meitzner, G.; Iglesia, E. *J. Phys. Chem. B* **2001**, *105*, 506−513.
(38) Lee, J. S.; Boudart, M. *Catal. Lett.* **1993**, *20*, 97−106.